symmetry

MDPI

Article

GEANT4 Simulation of the Gamma-Ray Total Absorption Facility

Chong Zou [1,2,*], Guangyuan Luan [1], Haotian Luo [1], Qiwei Zhang [1], Jie Ren [1], Xichao Ruan [1,*], Hanxiong Huang [1], Zhaohui Wang [1], Guozhu He [1], Jie Bao [1], Qi Sun [1], Xiaoyu Wang [1], Mengxiao Kang [1], Jincheng Wang [1], Yingyi Liu [1], Haolan Yang [1] and Xuanbo Chen [1]

[1] Key Laboratory of Nuclear Data, China Institute of Atomic Energy, Beijing 102413, China; luangy@ciae.ac.cn (G.L.); luoht2000@163.com (H.L.); zhangqw@ciae.ac.cn (Q.Z.); renjie@ciae.ac.cn (J.R.); huanghx@ciae.ac.cn (H.H.); mcwzh@ciae.ac.cn (Z.W.); heguozhu818@126.com (G.H.); baojie@ciae.ac.cn (J.B.); sunqi@ciae.ac.cn (Q.S.); xyw_ciae@outlook.com (X.W.); kangmengxiao2009@hotmail.com (M.K.); wangjincheng@imut.edu.cn (J.W.); lly_ciae@outlook.com (Y.L.); haolan_yang_ciae@outlook.com (H.Y.); xuanbo_chen@protonmail.com (X.C.)

[2] China Shipbuilding Trading Co., Ltd., Beijing 100044, China

* Correspondence: zouc@mail.chinaships.com (C.Z.); xichaoruancx@ciae.ac.cn (X.R.)

Abstract: To fulfill the needs of neutron capture reaction cross-section measurement in the keV energy region in the field of nuclear astrophysics and advanced nuclear energy system development, the 4π BaF_2 Gamma-Ray Total Absorption Facility (GTAF) developed by the Key Laboratory of Nuclear Data of the China Institute of Atomic Energy (CIAE) was transplanted and installed at the Back-streaming White Neutron Source (Back-n) of the China Spallation Neutron Source (CSNS) in 2019. A series of results has been achieved and published based on the GTAF since then, and it has been identified that the need of reducing backgrounds is becoming increasingly urgent. In order to understand the origins of backgrounds and to optimize the facilities, a detailed simulation program using GEANT4 toolkits was established and is presented in this paper. The symmetry in the geometric arrangement of the 4π BaF_2 detector array plays a critical role in ensuring uniform detection efficiency and accurate reconstruction of gamma-ray spectra, which is essential for neutron capture studies. To demonstrate the availability of the proven codes, several practical examples of assisting the process of experimental data and helping verify the optimization proposition are also shown in this paper.

Keywords: Monte Carlo simulation; gamma-ray total absorption facility; neutron capture cross section; GEANT4; geometry optimization; white neutron source

Academic Editor: Maxim Y. Khlopov

Received: 2 November 2024
Revised: 20 December 2024
Accepted: 27 December 2024
Published: 9 January 2025

Citation: Zou, C.; Luan, G.; Luo, H.; Zhang, Q.; Ren, J.; Ruan, X.; Huang, H.; Wang, Z.; He, G.; Bao, J.; et al. GEANT4 Simulation of the Gamma-Ray Total Absorption Facility. *Symmetry* **2025**, *17*, 92. https://doi.org/10.3390/sym17010092

1. Introduction

The Gamma-Ray Total Absorption Facility (GTAF) shown in Figure 1 is a sophisticated detector providing a critical consideration in the keV energy region with respect to neutron capture cross-section measurements [1,2]. These measurements are vital for the progress of nuclear astrophysics and the design of advanced nuclear reactors [3]. The GTAF proves especially useful for studying the neutron capture process in the stellar environment, which is most important for the understanding of nucleosynthesis within stars and also of great importance in improving precision in the designs of nuclear reactors, where neutron capture plays an important role in energy generation and waste management [4,5].

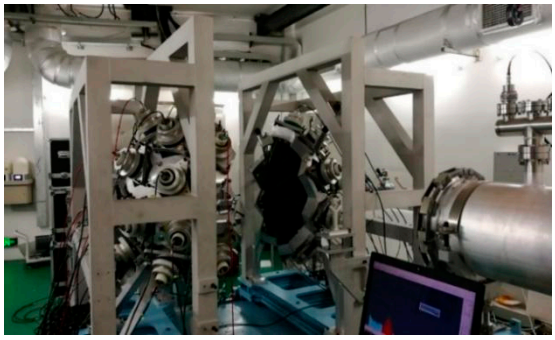

Figure 1. GTAF detector array and associated facilities installed in the Hall-2 of Back-n CSNS [6].

The GTAF was installed for the first time in 2019 at the Back-streaming White Neutron Source (Back-n) at the China Spallation Neutron Source (CSNS) [7]. It provides an advanced platform for detecting neutron-induced gamma-ray emissions, a key signature of neutron capture events [8]. The facility has large solid angular coverage and high detection efficiency, which are vital in performing gamma-ray emission measurements precisely [9,10]. Developing advanced optical techniques employing resonance-based techniques to enhance the sensitivity and suppress background noise would provide an excellent opportunity to optimize efficiency and spectral resolution in GTAF setups [10]. Developments in detector technology and materials and studies on the gamma radiation effects on superconductors, especially in superconducting tapes, as well as advances in avalanche photodiodes for accurate optical measurement, greatly add to the performance of a detector [11,12]. Innovations in energy-efficient designs and structural optimization techniques further align with the need for robust detection systems in high-radiation environments [13–15].

The Time-of-Flight (ToF) technique is crucial for distinguishing different neutron interactions and for measuring the neutron energy spectrum; it is well-suited for studies of neutron capture reactions in the low energy range [16,17]. The working principle of ToF is incorporated into some specific subdetectors within the GTAF facility, including scintillation detectors and neutron time-of-flight counters [18]. Those sub-detectors work as a team to provide high-precision temporal measurements, which in turn serve as a basis to evaluate the energy and properties of the captured neutrons [19].

The detector arrangement consists of a number of layers together engaged in capturing and measuring gamma rays from neutron capture reactions. The symmetric geometry configuration of the detector arrangement guarantees uniform solid-angle coverage and detection efficiency for all directions, which is vital to minimize systematic errors and achieve satisfactory accuracy in cross-section measurements. Advanced 3D modeling and reconstruction techniques, such as those used for complex geometries in lunar crater analysis, can inspire further refinements in simulating and optimizing detector configurations [20]. The GTAF accepts a design that makes it possible to accurately measure neutron capture cross-sections as well as to study neutron interactions at lower energies.

To facilitate the experimental data analysis, a detailed Monte Carlo simulation grid was built using the GEANT4 toolkit. This simulation modeled the interactions of neutrons and gamma rays through the GTAF to optimize the design of a detector and the data analysis procedure. Section 2 presents the setup and methodology of the simulations. Sections 4 and 5 present a comparison of the simulation results against standard libraries and against experimental data for verification purposes. In addition, Section 6 shows practical examples of how simulation can actually be used for both data analysis and for the optimization of the GTAF geometry against background interference.

2. Basis of GTAF Detector

2.1. Time-of-Flight Method

The Time-of-Flight (ToF) method is a commonly used method in measuring particles. It relies on the principle that the time it takes for a neutron to travel a known distance is inversely proportional to the square root of the neutron energy at low energies, which can be approximately calculated by Equation (1) [21].

$$E_n = \left(\frac{72.3 \times L}{t}\right)^2 \tag{1}$$

where t refers to the flight time, L to the flight distance, and E_n to the primary neutron energy.

The measurement of neutron flight time is designed for great accuracy using specific timing hardware and a software system, since it is crucial to determine the neutron's energy and to reconstruct the spectrum at the GTAF [22,23].

2.2. Multiplicities of (n, γ) Reactions

The multiplicity considered in the simulation mainly includes two sources, namely reaction multiplicity and response multiplicity.

It plays a key role in benchmarking valuable information about reaction channels and underlying physics process, such as elastic scattering, inelastic scattering, radioactive capture, etc., since each event has a distinctive multiplicity signature [24,25].

The reaction multiplicity is defined as the number of different de-excitation processes of the compound nucleus, which is produced after capture reactions occur between the neutron beam and the sample, as shown in Figure 2a. In simulations, it can be easily resolved, since all information can be recorded if appropriate simulated physical processes are designed.

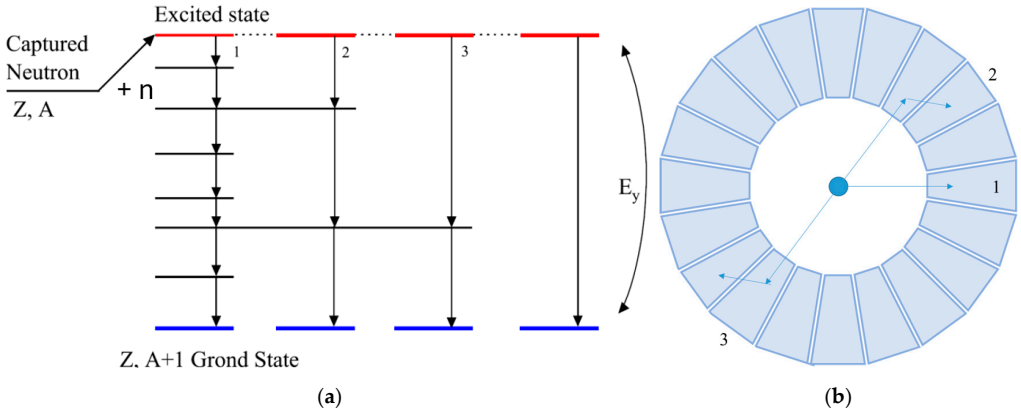

Figure 2. (**a**) Principle of isotope de-excitation: A captured neutron excites the nucleus, which de-excites through multiple gamma-ray emissions. (**b**) Schema of response multiplicity: gamma rays may be fully absorbed by one detector crystal (process 1) or undergo Compton scattering, triggering multiple crystals (processes 2,3).

The response multiplicity is defined as the number of detector crystals that respond and record the γ particles generated. Under ideal circumstances, the γ particles generated after the capture reaction occurs may respond and be absorbed on a single BaF_2 crystal, as seen in process 1 in Figure 2b. However, Compton scatterings might occur, causing the reaction signals to appear on multiple crystals, as shown in processes 2,3 in Figure 2b. In the simulations, this might be resolved by discriminating different geometric volumes with the help of the embedded interface of GEANT4, which is described in detail in Section 4.3.

2.3. Pile-Up Energy

For GTAF, the neutron capture reaction is of the most concern. To distinguish the neutron capture reaction, one of the most practical ways is to find the value of pile-up gamma-ray energy E_{ex}, since no matter how many reaction channels have been experienced, E_{ex} remains constant if all data can be detected and restored ideally, as shown in Equation (2).

$$E_{ex} = E_n + Q \tag{2}$$

where E_n refers to the neutron energy and Q to the reaction Q value.

As mentioned in Section 2.2, there could be multiple de-excitation reaction channels where capture reactions can occur in actual experiments, and two or more photons may hit the same BaF_2 crystal almost simultaneously. Since there is a limit of time resolution in the nuclear electronics of GTAF, the energy signals generated might be accumulated together, which appears as a high-energy peak in the spectrum (Figure 3). Problems are much easier to solve in the simulations since all event information can be recorded and the summation energy under different reaction channel conditions can be distinguished, as described in Section 4.3.

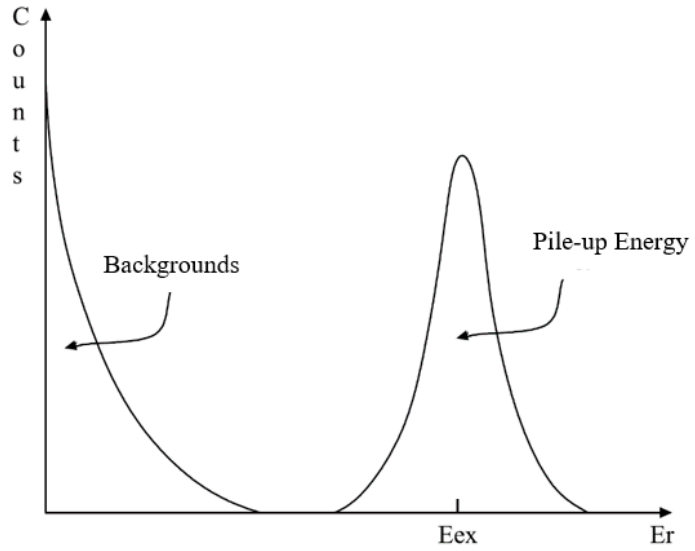

Figure 3. Principle of pile-up energy [6].

3. Monte Carlo Simulation

3.1. General Idea

3.1.1. General Design

As discussed in Section 1, a reliable Monte Carlo Simulation is needed to be established in order to fulfill the needs of the amelioration of facilities and to help in the analysis of the experimental data.

The reliability of the Monte Carlo simulation depends on the details of reconstruction in various parts, i.e., (1) detailed geometry reconstruction; (2) accurate physics configurations; (3) reasonable calibration and neutron beam sources; (4) a capable event reconstruction algorithm; and (5) a suitable digitization process.

The GEANT4 simulation toolkits package is chosen, as it has been widely used and verified in nuclear physics and high energy physics, with strong abilities of extensive physics configurations and mutual geometric reconstruction methods [26]. The kernel version of GEANT4 in use in the simulation of this paper is 11.1.2. The general working flow of the simulation is shown in Figure 4.

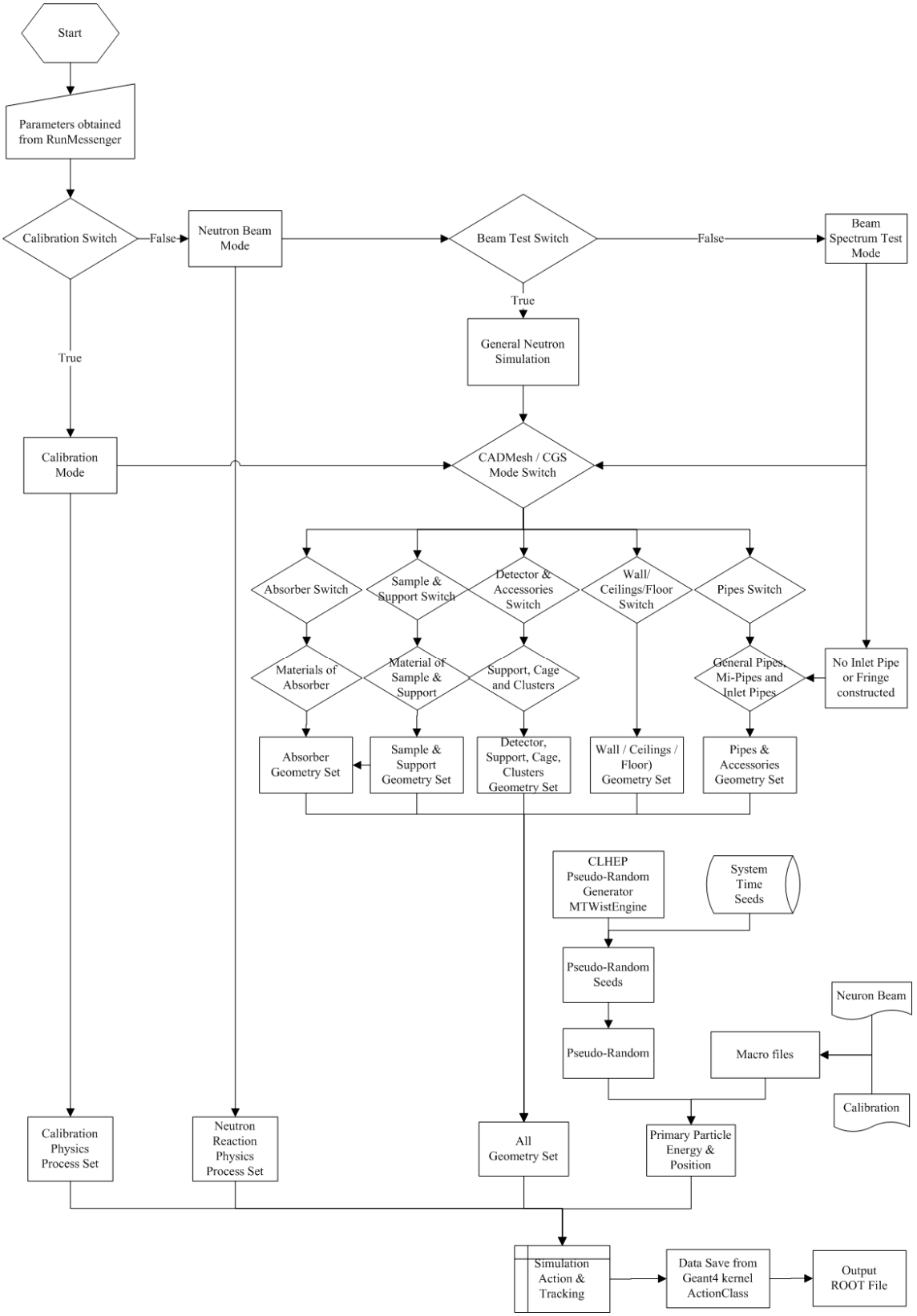

Figure 4. General data flow of simulation codes.

3.1.2. Simulation Modes

To adapt to different needs of geometry simulation under certain experimental conditions, different Boolean variables are offered to users in order to switch between different modes of simulation, including geometric constructions, physics models, and information digitization processes.

3.2. Geometry Reconstruction

3.2.1. Construction Methods

The geometry is reconstructed to have the most reasonable details. Apart from the mechanical fabrication errors, the geometric parameters and related materials of the facilities are set as the same as the ones measured directly from the actual arrangements [6] in the Back-n of CSNS.

In addition to using the Constructed Solid Geometry (CSG) method or the CSG-like methods embedded in GEANT4 toolkits, the subassemblies of the facilities are also reconstructed using the CADMesh method as a back-up and an agile option. The two mentioned methods are designed to be able to switch between one another via a Boolean variable switch [27].

The CADMesh is a valuable tool in reconstructing detector constructions in GEANT4 simulations. It allows importing complex geometries created in Computer-Aided Design (CAD) software version 2.0.3, with a support of various common ACSII format files, into the GEANT4 simulation program directly.

Although both CSG and CADMesh methods are based on computer graphics geometric logics, more preset basic graphics and logical calculation operations are provided by commercial CAD software version 2.0.3 when constructing elements, which offer the CADMesh method's possibility of rapidly building high-level accurate geometric volumes, ensuring that the simulation of the detector's physical characteristics can fulfill the crucial need for obtaining results in particle tracking. It is especially advantageous that the CADMesh method can easily excel at handling complex 3D shapes and curved surfaces when simulating detectors, such as for the GTAF series detectors, which contain quite a lot of intricate and irregular geometric elements.

According to the topologic definition of different fields in ACSII format CAD files, such as vertex positions, normals, mappings, etc., as created by CAD version 2.0.3, an interface program is used to read and translate parameters to ensure the core program of GEANT4 completes the corresponding geometric construction whereas the corresponding materials are defined subsequently in the same way as the CSG method in GEANT4 [28].

3.2.2. Geometry by Categories

The geometric simulation and some of the typical subassemblies are shown in Figure 5.

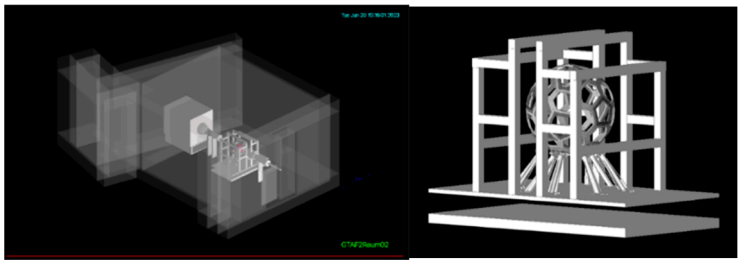

(**a**) (**b**)

Figure 5. *Cont.*

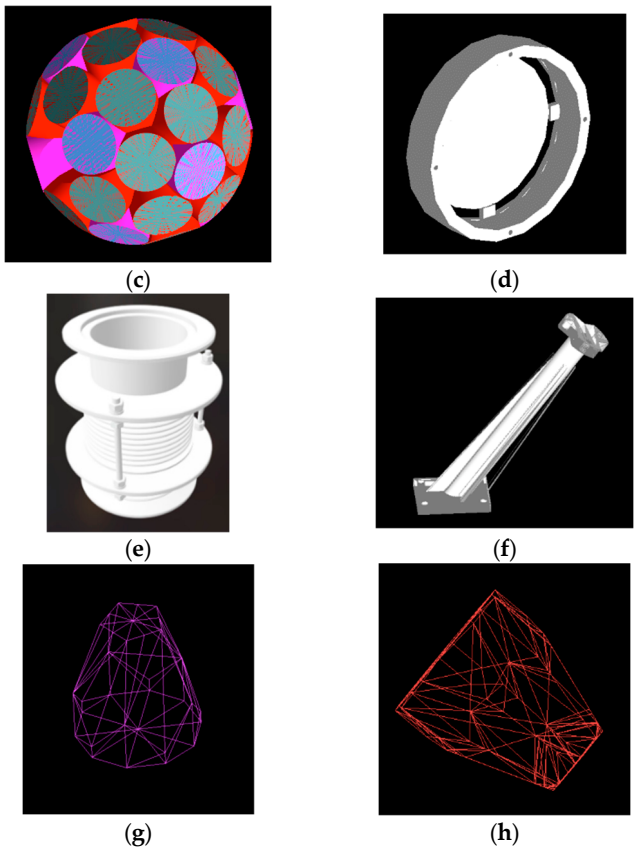

Figure 5. Typical simulation reconstruction. (**a**) Mass plan of the Hall-2 geometry using CSG + CAD method; (**b**) central zone for the detector and its associated geometry using CSG + CAD method; (**c**) BaF_2 crystal geometry using CSG/CAD method; (**d**) sample tray/support geometry using CSG/CAD method; (**e**) bellow geometry using CSG + CAD method; (**f**) cage support geometry using CAD method; (**g**) BaF_2 pentagonal pyramid; (**h**) BaF_2 hexagonal pyramid.

In order to facilitate simulation and analysis, geometric structures are constructed according to regions, as described below.

a. **Walls**

The wall category includes three major subcategories: side walls, ceiling, and floor. The geometric dimensions of the structure are completed based on the design drawings, with local details adjusted according to the actual layout conditions.

Considering that particles may be partially scattered after passing through the particle dump and re-enter the experiment hall, and that the structure at the rear of the beam line (open stairwell, etc.) might affect the trajectory of the particles, special consideration was given to structuring the stairwell and other parts behind the experimental hall.

b. **Pipes and Dump**

The particles complete the transportation in the vacuum pipeline. The pipeline and its support legs should be reconstructed as much as possible according to the drawings in the simulation, since they are the parts with direct contact with the primary particles. In order to facilitate the research of different environment effects (under vacuum and air conditions), the inner volume of the pipeline is specially constructed as a separate geometry. A Boolean switch to change the material (vacuum or air) is preset, as shown in Section 3.1.2.

Meanwhile, considering that under the calibration mode, the upstream vacuum pipeline that penetrates the wall has little impact on the simulation results, this very

pipeline as well as other wall-piercing structures would be no longer constructed when the calibration mode is selected by the user in order to improve the efficiency.

For relatively complex geometries such as bellows, quick-release flanges, and pipeline support legs, the CSG method is mainly constructed by volume-equal geometric conversion coefficients (more details in Section 3.2.3), while in the CADMesh mode, it is completely reproduced according to the design drawings, as shown in Figure 5e.

c. **Detector and Accessories**

The simulation of the detector and its accessories is based on the geometry of the actual detector, as shown in Figure 5b.

The BaF_2 crystal is constructed based on the pentagonal pyramid and hexagonal pyramid structure, which is established with cylinders and plates, as shown in Figure 5g and 5h, respectively. An assembled array is shown in Figure 5c. Outer covering layers, including the black tape light-shielding layer (Kapton material) and the aluminum shell were also simulated and were consistent with the actual manufacturing size and layout. In order to avoid the floating-point number overflow that may occur when constructing geometry in GEANT4, a slight gap of 0.01 mm is placed between the two layers.

While constructing some of the complex geometries, such as the detector support legs, detector gantry, and sample support/tray, the geometric construction is reconstructed through volume-equal geometric conversion coefficients (more details in Section 3.2.3), as shown in Figure 5d,f.

However, as for the moving mechanism of the support platform of the detector, no detailed simulation was performed, since it is considered that the entire structure is located below the support platform, which has a certain local effect on particle scattering but has little impact on the overall effect.

d. **Functional Virtual Geometric Area**

Considering the need to verify the simulated geometric cross-section and energy spectrum of the incident neutron beam, a functional virtual geometry is set up in the through-wall vacuum pipe. The designed size of the set virtual geometric area is the full pipeline inner cross-section with its material vacuum.

3.2.3. Construction Parameter Design

As mentioned above, volume-equal geometric conversion coefficients and material composition conversion coefficients are used in order to ensure the efficiency of the simulation.

a. **Volume-equal Geometric Conversion Coefficient**

For certain elements whose local geometric effect is no need to be detailed considered, the related parameters are calculated and set by volume-equal geometric conversion coefficients under the CSG mode. The simulated converted geometric coefficients of each main structure in CSG mode are shown in Table 1.

Table 1. Typical volume-equal geometric conversion coefficients in CSG mode.

Category	Volume	Sub-Assemblies	Geometry	Coefficients
Environment	Door LM1822	Concrete Inside Door	Cube	0.97
Environment	Door LM1822	Cover of Door	Cube (Logic Subtraction)	0.03
Pipeline	Bellow Type BP300	Bellow Outside	Cylinder (Logic Subtraction)	1.47

Table 1. *Cont.*

Category	Volume	Sub-Assemblies	Geometry	Coefficients
Pipeline	Bellow Type BP300	Bellow Inside	Cylinder (Logic Subtraction)	0.96
Pipeline	Quick-Release Flange Type KF100	Flange	Cylinder (Logic Subtraction)	1.24
Pipeline	Quick-Release Flange Type KF100	Flange Inside	Cylinder (Logic Subtraction)	0.96
Pipeline	Support Leg for Pipe	Support Leg for Pipe Type P100	Cube (Logic Addition)	0.82
Detector	Detector Support Legs	Detector Support Legs	Cylinder (Logic Addition)	1.12
Detector	Support Platform of Detector	Support Platform of Detector	Cube (Logic Addition)	1.14
Detector	Light-Shielding Layer	Light-Shielding Layer	Volume (Logic Subtraction)	1.12
Detector	Sample Support	Sample Support	Cylinder (Logic Addition)	1.06
Dump	Absorber	Absorber Inside Dump	Cylinder (Logic Addition)	0.71

b. **Material Composition Conversion Coefficients**

Simulated materials are reconstructed according to the test results provided by the manufacturer or the average composition values of the corresponding National Fabrication Standards, as shown in the Table 2.

Table 2. Typical material composition conversion coefficients.

Category	Volume	Description	Material
Environment	Walls	Concrete	Standard Concrete
Pipeline	Stainless Steel	High-Carbon Steel	Mean Value GB 1220-92 and GB/T 11253-2019
Pipeline	Stainless Steel	Stainless Steel Type Q235	Mean Value GB 1220-92 and GB/T 20878-2007
Pipeline	Stainless Steel	Stainless Steel Type 304	Mean Value GB 1220-92 and GB/T 20878-2007
Pipeline	Aluminum	Aluminum Alloy Type 6061	Mean Value GB/T 3191-2019 and GB/T 3880.2-2012
Dump	Absorber Layer Inside Dump	B4C	Material B4C
Dump	Absorber Layer Inside Dump	Polyethylene (Boron Carbide)	Customized Reconstructed Due to Different Percentage of Boron Carbide
Detector	BaF_2 Crystal	BaF_2 Crystal	BaF_2
Detector	Light-Shielding Layer	Black Tap	Kapton
Detector	Boron Glass	Boron Glass	Pyrex Glass

3.3. Physics Models

3.3.1. Physics Model Selection

It is crucial to select appropriate physical models. Two different physical packages are designed in order to fulfill the needs of two different simulation modes selected by users, e.g., the Calibration mode and the Neutron Beam mode.

a. **Calibration Mode**

The simulation process of the Calibration mode is mainly to verify the reliability of the geometric reconstruction. Three γ sources are simulated as calibration sources as in the experiment, where elastic scattering, inelastic scattering, and the decay process using G4DecayPhysics, G4RadioactiveDecayPhysics, G4IonElasticPhysics, G4IonPhysics, G4EmStandardPhysics, and G4EmExtraPhysics (GEANT4 Simulation Toolkit, CERN, Geneva, Switzerland) are considered in the simulation.

b. **Neutron Beam Mode**

Compared to the Calibration mode, greater consideration is given to the response in low energy range in the Neutron Beam mode.

Since different physical packages concern different ranges of energy, basic hadron physics packages, including QGSP, BIC, BERT, FTFP, and QBBC, are tested, some of which are shown in Figure 6. Neutron elastic scattering, inelastic scattering, fission, decay, and neutron capture physical processes using G4IonElasticPhysics, G4IonPhysicsXS, G4StoppingPhysics, and G4DecayPhycics and neutron physics models including G4NeutronHPElastic, G4NeutronHPinelastic, G4NeutronHPFission, and G4NeutronHPCapture models are designed to be used in the physical models. The interactions between γ particles and particles are well defined and processed by the G4EmStandardPhysics (option 4).

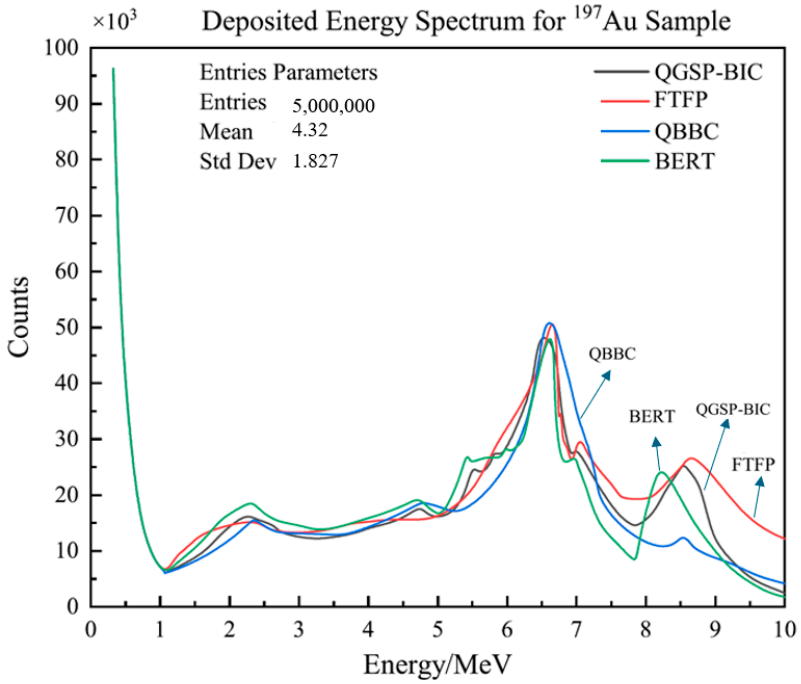

Figure 6. Deposited energy spectrum under different basic physical models.

Among different physics packages, it can be seen that the QGSP_BIC preset physics package responds with more accurate peaks, including peaks of the Q values of different isotopes, several slight escape peaks, and the neutron capture characteristic peak of ^{197}Au.

This was chosen because, with high-quality cross-section data, this model is efficient for neutron capture reactions at low energies (<20 MeV). As shown in Figure 6, it closely fits the gamma-ray peaks for isotopes like ^{197}Au.

Electromagnetic processes, e.g., Compton scattering and photoelectric effects, were accomplished with the EMV_option4 application to give realistic gamma-ray interactions and pile-up energy spectra.

Neutron capture and pawing interactions were simulated using G4NeutronHP and G4IonPhysicsXS, which are crucial for calculating the background and for slow neutron transport. Comparison with other models verified QGSP_BIC_HP as the most accurate for studies related to low-energy neutron capture.

In addition, in order to deal with the cross-section parameters in the low energy range, an interface that references LEND (for energy under 20 MeV) and a specific "HP" package and option 4 of the electromagnetic interaction package are used, with some of the cascade parameters and reaction parameters adjusted [29]. The refinement and customization of the physical simulation process of GTAF continues to be studied and developed. The current results are shown in Section 5 in this paper.

3.3.2. Physics Process Design

The preliminary applied physics processes and models are shown in Table 3. They will be continued to be refined in subsequent work due to the different needs of simulation.

Table 3. Applied physics processes and models.

Physics Model	Mode	
	Calib	Neutron
QGSP_ BIC_HP	■	■
EMV_option4	■	■
DecayPhysics	■	■
BiasedRDPhysics	■	
HardronElasticPhysicsHP	■	■
IonElasticPhysics	■	
IonPhysics	■	
GammaNuclearPhysics		■
GammaNuclearPhysicsLEND		■
NeutronHPPhysics		■

During the simulation process, different cut and kill threshold parameters were set for different simulation conditions.

For the Calibration mode, the default step length for gamma, e−, and e+, at 1 mm, is preset, since it is only used to verify the validity of the geometric model.

Considering the Neutron Beam mode, different kill and cut thresholds are set according to different simulation modes, such as the discriminating reaction channel mode and debugging mode, and according to the different conditions in which different physical processes occurred. In the overall settings, the lower limit of energy is set to 0.9 eV, and the upper limit is set to a sufficiently high one, namely 20 GeV in this simulation. Meanwhile, the lower limit threshold is set to 0.99 times the default HP models when it comes to the neutron capture physics process. The QGSP_Model_1 is registered with parameters referenced to the experimental data for the hadron inelastic physics model.

In addition, since the cross-sections of most nuclides in the library that comes with GEANT4 are only average values, a program based on the DiceBox is used to define the reaction cross-sections of the specific isotopes concerned [30].

3.4. Primary Sources

Two types of sources, i.e., (1) calibration sources of ^{60}Co, ^{137}Cs, and ^{22}Na; and (2) neutron beams, including (a) neutron beams output from Back-n and (b) 4.9 eV mono-energetic neutron beams, are reconstructed using specific macro files, which contain a histogram of spectral and spatial parameters and related normalized weighting coefficients to provide the required information for the simulation of primary sources.

The initial particles are designed and implemented by the General Particle Sources (GPS) method in GEANT4. Basic information of the initial particles, such as energy spectrum and geometric spatial distribution, in different calibration sources and neutron beams are designed in an independent macro file, which can be called through the interface program that comes with GEANT4 to assign parameters to the initial particles in the simulation.

3.4.1. Source Simulation

a. **Calibration Sources**

The three Calibration Sources of ^{60}Co, ^{137}Cs, and ^{22}Na are reconstructed in the simulation, with the geometric parameters the same as in real experiments [31]. In the called macro files, geometric parameters of the calibration sources are set to ϕ 32 $\times$ 4 mm, ϕ 32 $\times$ 4 mm, and 25 $\times$ 25 mm, respectively, with an initial kinetic energy equal to 0 and a two-dimensional geometric isotropic distribution.

b. **Neutron Sources**

Two neutron beam sources, mono-energetic neutron beams and spectral neutron beams, are simulated.

Due to the time-resolution limit of hardware in real experiments, the Time-of-Flight (ToF) spectrum of beams with an initial energy over 1 MeV cannot be well resolved. Therefore, in the first stage of simulation, an upper energy limit of 1 MeV is set for both of the options [31].

In the called macro files, the spectral distribution of initial particles is simulated with the same spectral and spatial characteristics from the Back-n beamline [32,33]. The z-axis coordinate of the neutron starting point is set to be -75.83 m. The starting x-axis and y-axis coordinates of each Event are sampled from the CMOS-measured Back-n beam profile distribution according to the x-axis position-weight and y-axis position-weight tables in the macro file by sampling with a weighted coefficient calculated using the clock pointer as the initial value of the pseudo-random number generator (PRNG). The simulated beam spot obtained at the entrance of the incident pipe in Hall 2 is shown in Figure 7.

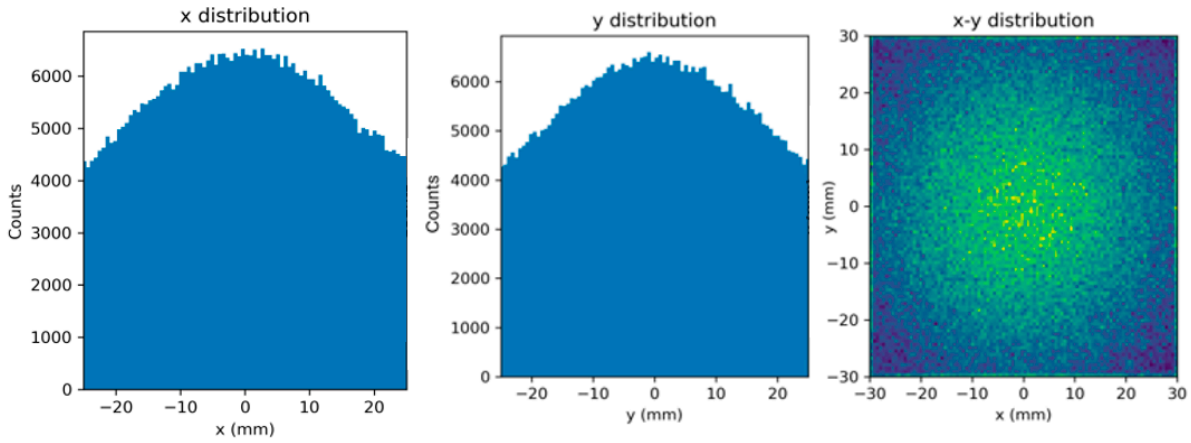

Figure 7. Simulation of neutron beam spot at Back-n of CSNS.

a. The mono-energetic neutron beams are simulated with parameters of a 4.9 eV mono-energy and a spatial beam spot obtained as mentioned above. This is used for obtaining a clear image of the largest resonant cross-section of the standard ^{197}Au sample, which leads us to verify the reliability of the codes and is used to help calculate the theoretical efficiency or other required information.
b. With a similar method, the initial kinetic energy emitted from the spectral neutron beams of each event is determined to be selected from the measured Back-n beam line source energy distribution table in the called macro file sampling, with the same weighted coefficient as used to obtain the spectral parameters. This kind of simulating beam is used for the analysis of backgrounds and for the calculation of the theoretical neutron capture cross-section of samples.

3.4.2. Pseudo-Random Number Generator

The statistical properties of PRNGs have a great impact on the reliability of Monte Carlo simulation results. There are several popular candidate PRNGs for nuclear physics, such as the James Random, Mersenne Twister, and Ranlux64.

The MTWistEngine pseudo-random number generator is chosen as the PRNG used in the simulation due to two main reasons, as follows:

(1) A big enough pool of valid pseudo-random number of $2^{19937} - 1$ can be generated in one single operation, which can support the needs of an upper limit of about 2×10^9 events in each run in GEANT4 toolkits and can also fulfill the potential needs for further study using the accumulated simulation data [34].
(2) A high reliability is achieved, since it has passed almost all the rigorous random number tests referred to the analysis thesis in reference [35].

In order to obtain the system beepers via an I/O data channel as initial seeds feeding the pseudo-random generator, a time seed interface program is designed, programmed, and linked to the EventAction class of the simulation program.

3.5. Simulation Run and Action Classes

Whether using the Calibration mode or the Neutron Beam mode, the simulation can be started by emitting the primary particles by calling up the detail parameters of the initial particles in the macro file (including the initial energy, initial momentum, and initial position) and the specific operation mode defined in the RunMessenger interface, via the GPS function embedded in GEANT4, as mentioned in Section 3.4.

After emission, the behavior of particles depends on the different physical models and definitions of the physical processes while travelling through various spatial volumes in the geometry described in Section 3.2, and they act to cut off or truncate the information according to the demands in the various action classes.

As mentioned in Section 3.1, different Boolean variable switches are coded to fulfill the needs of different simulations, based on which, two information acquisition modes are provided to users: the ***Stepping Acquisition Mode*** and ***Sensitive Detector Acquisition Mode***.

For simulations with a clear focus on certain geometric regions, the ***Sensitive Detector Acquisition Mode*** can be used to record the response. For instance, when we aim to analyze the pile-up energy in the detectors, an AssemblyLogicVolum, including all crystals and accessories, is defined as the SensitiveDetector; whenever the deposited energy is not equal to 0 in the Sensitive Detector, there is a Hit, with all required information recorded.

For simulations aimed at more broad research, the basic ***Stepping Acquisition Mode*** is activated, since all information happening in the world of simulation needs to be recorded for further analysis.

4. Primary Data Analysis Program

In order to meet the basic pre-processing requirements of the simulation data, a general data processing program with a set of Qt-based GUI interfaces is designed and tested.

4.1. GUI Interface

In order to facilitate the implementation of commonly used data preliminary processing functions, a visual human–machine GUI interface through Qt version 5.9.7 is designed, as shown in Figure 8.

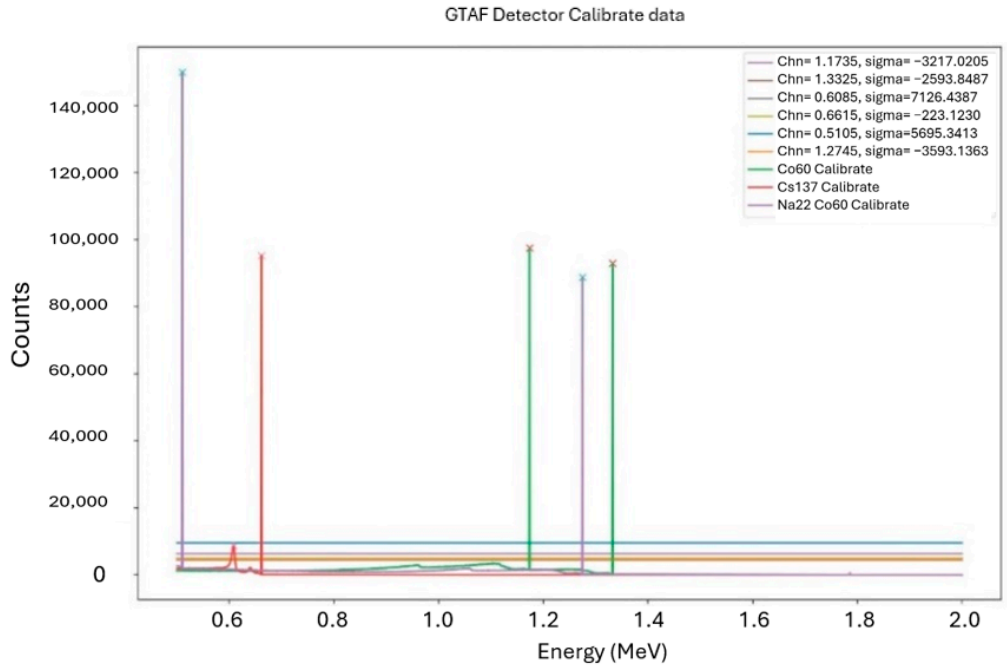

Figure 8. GUI interface of GTAF simulation pre-processing program.

Through Python Qt Version 5.15.11 and Py Root version 6.34.00, the commonly used functions are realized by transporting the data flow via various interfaces, including the import and export of files in various basic formats, switching between neutron beam mode and calibration mode as well as the display and fitting functions of the energy spectrum and ToF spectrum.

The visualization program uses the control of Qt and realizes the data interface required to call the above functions, realizing the basic data preliminary processing,

4.2. Event Cascade Algorithm

The simulation can be performed for each event or each run, as required. Consistent with the process of experimental data processing, two general and basic event reconstruction algorithm subprograms in the data processing program are designed: energy reconstruction and position reconstruction.

The reconstruction is relatively simpler in the simulation, since it is possible to retrieve the target data directly from GEANT4 built-in functions. Particles are transported and tracked via the functions of Action Classes in the framework of GEANT4 toolkits until they are absorbed in certain volumes or escape the set cut-off areas.

The essential values, such as the deposition energy, the time of flight, the multiplicities, the geometric volumes, the material, the reaction channel, and other relevant information, can be observed and recorded after each step or event. Meanwhile, the corresponding data

of each reaction channel can be distinguished by calling up the physics model or physics process of each track.

4.2.1. Pile-Up Energy Simulation

The deposited energy can be traced in each step of particle transportation with the help of the built-in algorithms of GEANT4, which is one of the privileges of processing simulation data compared to experimental data, with the pile-up energy peaks and event cascade reconstructions being much easier to complete.

The particles are designed to be transported via the functions of action class in each step until they are absorbed in certain volumes or exceed the preset cut-off areas. While the simulation runs, each particle will be labeled by each generation, and the associated information of particles is transferred via a user-set personalized function to the TrackingAction class in order to be further processed.

Considering that the simulation results of interest are those with responses in the detector array, the geometric volume information is of more importance. Therefore, a label for each volume number (the CopyID) is recorded at the same time.

For situations where further processing of energy deposition is not required, the above-extracted data can be directly transferred from the SteppingAction class to the EventAction class so as to be accumulated and stored directly, after which the data is finally passed to the Analyzer for saving in a certain format according to the designed dataflow as shown in Figure 4.

On the other hand, where there is a need for further processing, a TrackingAction class retains interface functions for users to filter the specific required deposition energy. According to the needs of the user's simulation objectives, data can be transferred to the Analyzer after preliminary processing in the TrackingAction class, where more preprogrammed reorganization tools, such as different reaction channels, different multiplicities, and different areas to store and construct the required energy spectrum, are set as described in Section 4.3.

The original simulation data output from the dataflow above are saved by separate detector crystals. The reconstructed energy spectrum can be output directly in the form of divided crystals, or according to the user's needs, a deposited energy spectrum reconstruction output in the unit of the total detector can be achieved in the form of the sum of the total deposition data of each crystal in the same Event.

The above functions can be implemented in the RunMessenger by adjusting relative Boolean variables or through GUI tabs. Thus, after each Run, the energy spectrum of particles can be reconstructed.

4.2.2. Time-of-Flight Spectrum Simulation

In order to verify the results with experimental data, the flight time of particles is designed to be recorded in the simulation.

The start time point T0 is preset in the EventAction class at the beginning of the Event, when the primary particles begin to emit in every loop. When triggered in each Step (under SteppingAction mode) or in each Sensitive Detector zone (under SensitiveDetector mode), the corresponding time is recorded and saved in a tuple or histogram predeclared in the RunAction class. Note that the recorded time mentioned above is a Global Time in the entire Event, since T0 is the beginning of each Event. Right at the end of each Event, the corresponding time data are recorded in different tuples or trees in the ROOT files through the pre-selection conditions in the action classes of each Step, Track, Stack, or Event. Therefore, a ToF Spectrum can be generated at the end of the whole Run, e.g., the end of the final Event.

In addition, similar to the processing of experimental data, the corresponding simulated energy spectrum (E-ToF) can be calculated using the flight length of particles, and the simulated ToF spectrum by using Equation (1). The flight length of particles is obtained by adding the flight distance in each Step. It is calculated in the geometric simulation program and transferred to the analysis functions by the two following ways, which can be switched by users through a Boolean variable.

(1) Calculation by extracting the geometric length of the corresponding passing geometric elements in the Detector Construction source file; the geometric parameters are transferred to the Analyzer source file through the transfer function.
(2) Calculation directly in the Step action class through the built-in variable function of the GEANT4 toolkit, whereafter the step length is passed to the function in the Event action class in order to store and generate the E-ToF spectrum directly.

4.2.3. Position Reconstruction

Similar to the reconstruction of the ToF spectrum, the position information (three-dimensional vector tuple) of each step can be traced and recorded, while the deposited energy (the difference between the pre-step and post-step energy) in dedicated geometric volumes is not equal to zero in the SteppingAction class.

4.3. Reorganization Tools

4.3.1. Discrimination of Multiplicity

As discussed in Section 2.2, a proper design should be considered for the processing and identification of the multiplicities.

For the reaction multiplicity, the embedded interfaces, which offer a method to obtain the physics process in each step, can help to discriminate and record the multiplicities for further study via data processing tools; the ROOT program is used in this paper.

An algorithm is designed to simulate and record the response multiplicities, where, technically, the number of different CopyIDs of geometric volumes where the deposited energy is not equal to zero before the particle is fully absorbed or escapes from the sensible arrays is seen as the theoretical response multiplicities, since there is a unique CopyID tagged to each of the geometric volumes reconstructed in the simulation. Depending on whether two successive responses occur on adjacent crystals, response multiplicity is defined as cluster multiplicities or crystal multiplicities.

Examples of tools for discriminating and recording multiplicities and the use of multiplicities obtained as tools for further analysis of the data are presented in Section 5.1.

4.3.2. Reaction Channels

In experimental data processing, distinguishing data from different reaction channels is the core algorithm of data processing, which is realized through different gates in order to help understand the experimental data and phenomena.

In simulation, the physical process occurring at each step can be traced before or after each step. In order to avoid the null Pointer error in the C++ coding environment, apart from the usual protection by a judgement function, the post step physics model filter is used in this program. A string value, with a preset in GEANT4 or by a user-set dedicated physics model or physics process due to the Boolean value switch as chosen in the RunManager, would be returned. After transfer to the Stack and Track classes of the simulation program, the string values of the relevant physics processes or physics models are passed to the Analyzer and stored in the corresponding tuple or other format in a ROOT file.

After the simulation is completed, the value of the physics processes or physics models could be called in the Primary Data Analysis Program, and the ToF spectrum or energy spectrum involved in different reaction channels can be classified and plotted.

4.4. Spectrum Smearing and Semi-Automatic Peak Finding

4.4.1. Energy Spectrum Smearing

Since GEANT4 cannot simulate the nuclear electronic effect in the preset physical process, the ratio of electronic response is obviously 100%. Thus, the simulated data need to be broadened before supporting the experimental data analysis.

In the preliminary analysis program, the Gaussian function is used as the broadening algorithm. The specific process of the broadening algorithm is as follows:

(1) Determine the total normalized bin number and the corresponding coordinate value of the corresponding spectrum (or the corresponding segment of the spectrum);
(2) Determine an energy resolution that is set according to the experiment or set by the user;
(3) Determine the width of the error limit;
(4) Determine the constant of Gaussian broadening by ensuring that the integral of Gaussian broadening with the above parameters is the same as the original count value.

Plot and record the parameters.

4.4.2. Semi-Automatic Fitting and Peak Finding

Spectrum fitting and peak finding are generally performed in the range of interest when processing data. The semi-automatic spectrum fitting and peak finding process can be implemented in the primary data analysis program.

The algorithm of spectrum fitting and peak finding is similar to their counterpart of energy spectrum broadening, which is also achieved by fitting with the Gaussian function a series of basic initial parameters, including the approximate region of the peak position, basic fitting adjustment parameters, etc., that can be modified and fitted directly in the GUI interface mentioned in Section 4.1.

The peak position and the final coefficient of the fitting iteration will be displayed in the display area of the GUI interface or be printed in the Terminal, which will be stored and be used for subsequent data analysis.

5. Validation of Reliability

5.1. Responses to Calibration Source

The three calibration sources mentioned in Section 3.4 are designed to validate the reliability of the geometric simulations and the algorithm of reconstruction. The results are shown in Figure 9, in which the peaks of piled-up deposit energy are all in good agreement with the expected data, which demonstrates the reliability of the geometry and physics configurations.

In addition, the preliminary processing of multiplicities and reunited-BaF_2 crystals event plotting is performed for the simulation data. Taking the simulation data of ^{60}Co source calibration as an example, two gamma rays, with an energy of 1.17 MeV and 1.33 MeV, respectively, emit spontaneously. The pile-up energy of 2.5 MeV can be a benchmark to evaluate the efficiency of the detector array, as discussed in Section 2.2 and shown in Figure 10.

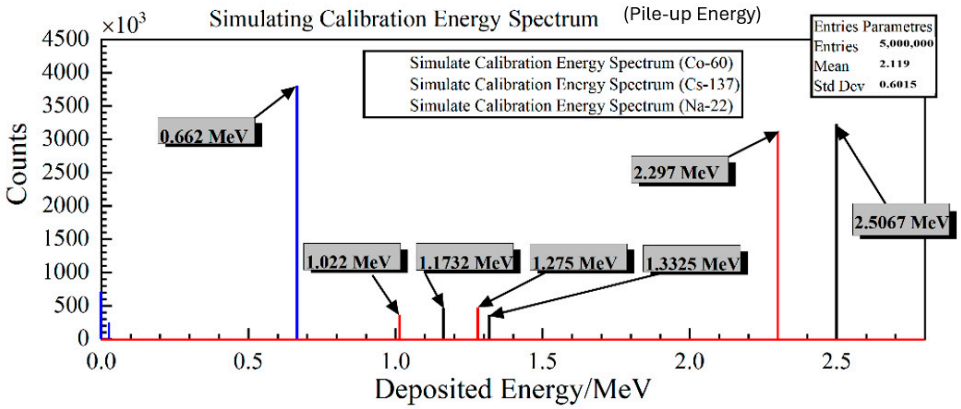

Figure 9. Simulated calibration energy spectrum (pile-up energy) for different sources. The blue line represents ^{137}Cs, the black line represents ^{60}Co, and the red line represents ^{22}Na.

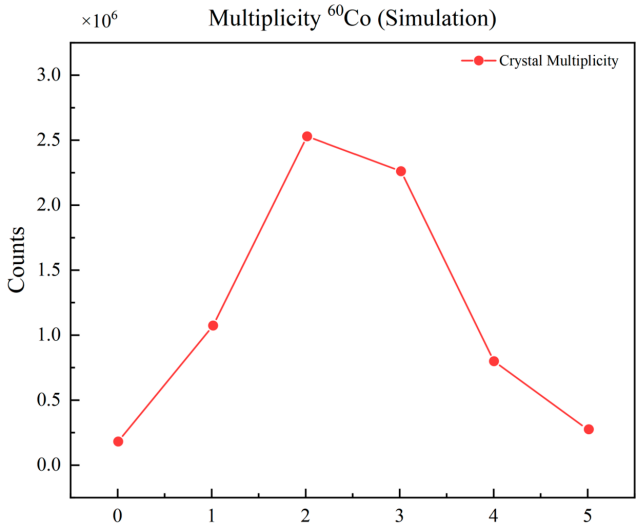

(**a**) Simulated multiplicity distributions of ^{60}Co source

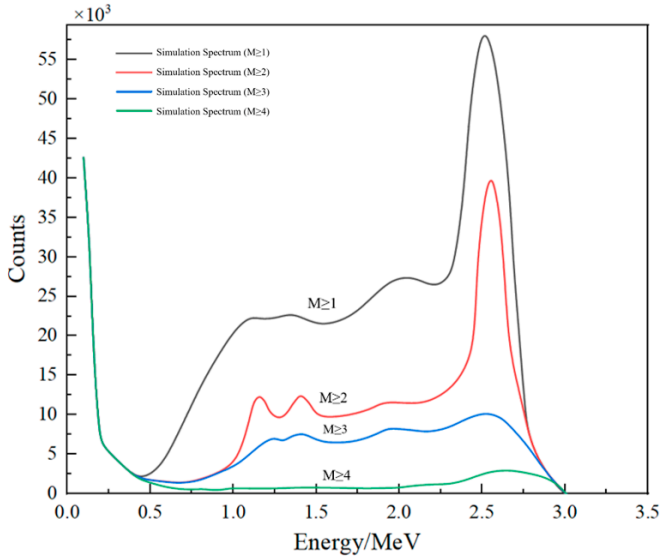

(**b**) Energy spectrum in different multiplicity filters conditions

Figure 10. Demonstration of multiplicity identification for ^{60}Co source simulated calibration experiment.

It can preliminarily be proven that the geometric reconstruction of the simulation program is effective, with the basic reconstruction algorithm available. At present, the

experimental data processing of GTAF is still ongoing, and the results from the experiment will be published in the future.

5.2. Response to Neutron Capture Reaction

Considering that there is a very large resonant neutron capture cross-section at 4.9 eV of the isotope ^{197}Au, which is several orders of magnitude larger than other cross-sections, such as elastic scattering, the very specific monoenergetic neutron beam is used for verifying the physics configurations of the simulation.

To this end, a 4.9 eV monoenergetic neutron beam with the same geometric spatial distribution as the Back-n neutron source starts from the vacuum tube, 72.7 m away from the sample tray, and a standard thin cylindrical ^{197}Au Sample with the same geometric dimensions as the experiment, i.e., a thickness of 0.2 mm and a diameter of 40 mm, is simulated.

In this simulation, a lower energy threshold of 10^{-2} eV is preset for each simulated crystal unit to facilitate preliminary data processing. The response information of particles on the BaF_2 crystal was recorded as described in Section 4.2, after which the energy spectrum and ToF spectrum were output through event reconstruction.

As shown in Figure 11, a peak of deposited energy around 6.51 MeV and a typical time peak of 2.478×10^6 ns are clearly shown in the Energy Spectrum and in the ToF Spectrum, respectively, which are consistent with the expected values and demonstrate well the validation of the simulation codes.

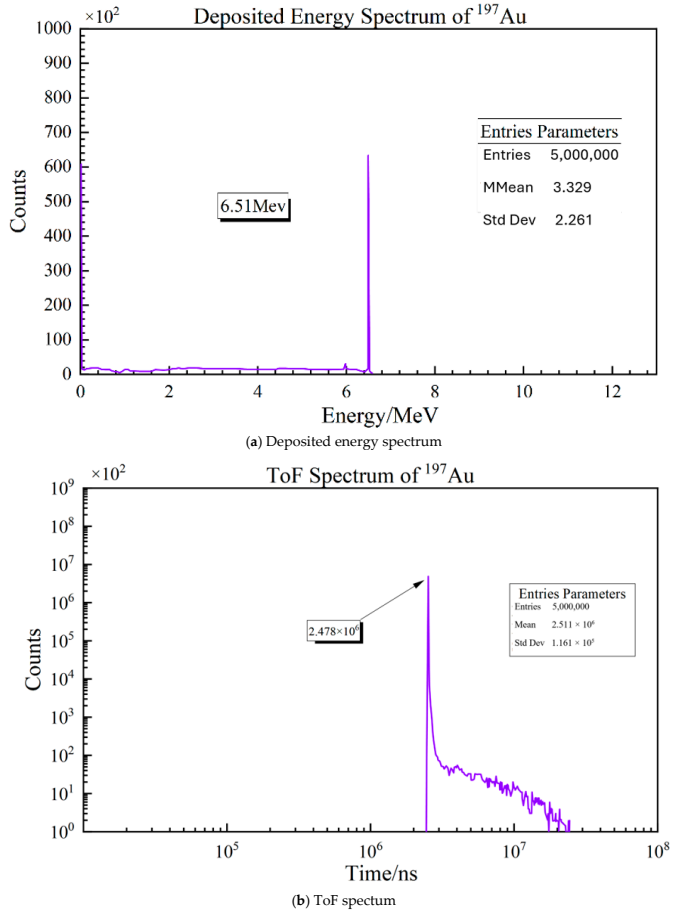

(**a**) Deposited energy spectrum

(**b**) ToF spectum

Figure 11. Simulation results of ^{197}Au sample response to the 4.9 eV monoenergetic neutron beam.

6. Practical Examples

6.1. Assistant Processing and Understanding Experimental Data

6.1.1. Leveraging GEANT4 Simulations for Experimental Data Analysis

The Monte Carlo simulation tool built around GEANT4 assists in analyzing and understanding experimental data. On one hand, the Monta Carlo tool can provide the experimental spectra of other neutron energies to assist in understanding neutron energy and reaction cross-section relationships. On the other hand, simulated results can help to understand the response of different components of the detection system to the reaction, to propose and verify the optimization proposition for facilities and to develop specific processes for data processing.

Background sources, such as scattered gamma rays and environmental neutrons, were identified by simulation so that specific alterations could be done, such as optimizing shielding placement and tweaking detector geometry as appropriate. These changes worked to reduce the background noise that hindered the performance of the GTAF experiment, thus enhancing its measurement quality.

6.1.2. Impact of Different Neutron Beam Energies

In order to speed up the simulation and considering the (n, γ) cross-section in real experiments, a Back-n neutron energy below 1MeV is often used as the input neutron source.

However, neutron beams in different energy regions may have different effects on the background. To confirm the influence of the high-energy part on the interested energy region, four different initial input neutron sources are simulated, with the Effect–Background Ratio results shown in Table 4.

Table 4. Theoretical Effect–Background ratio under different simulation beam conditions.

Number of Simulations	Neutron Beam Condition		Effect–Background Ratio
	Energy Spectrum	Spatial Structure	
N_04	Back-n Energy Spectrum (filter under 1 MeV)	Back-n Spatial Structure	7.26%
N_29	Back-n Energy Spectrum	Back-n Spatial Structure	7.11%

As can be seen from the above table, although the high-energy neutrons have a certain influence on the spectral structure, they have little effect on the key data, such as the back-ground–effect ratio. Therefore, when using simulation for rough analysis, a simplified neutron source term, with a filter of under 1MeV of energy, can be used to improve the computational efficiency.

6.1.3. Discrimination Data by Different Reaction Channels

The discrimination of different reaction channels is one of the benefits of using the simulation codes, since it can provide an ideal panorama of all the reactions occurring. A demonstration of this function is shown in Figure 12.

These simulations can help to estimate the detection efficiency of neutron capture reaction measurement. In addition, it is an important analysis tool to provide possibilities to help better understand the phenomena of experimental data and optimize the structure to reduce the background impact.

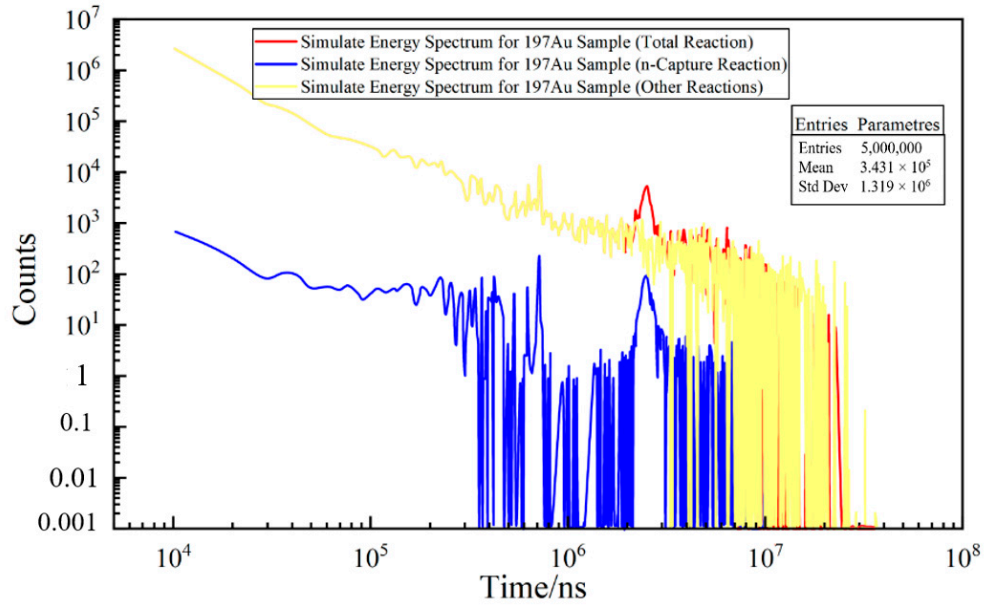

(**a**) ToF spectrum (different reaction channels)

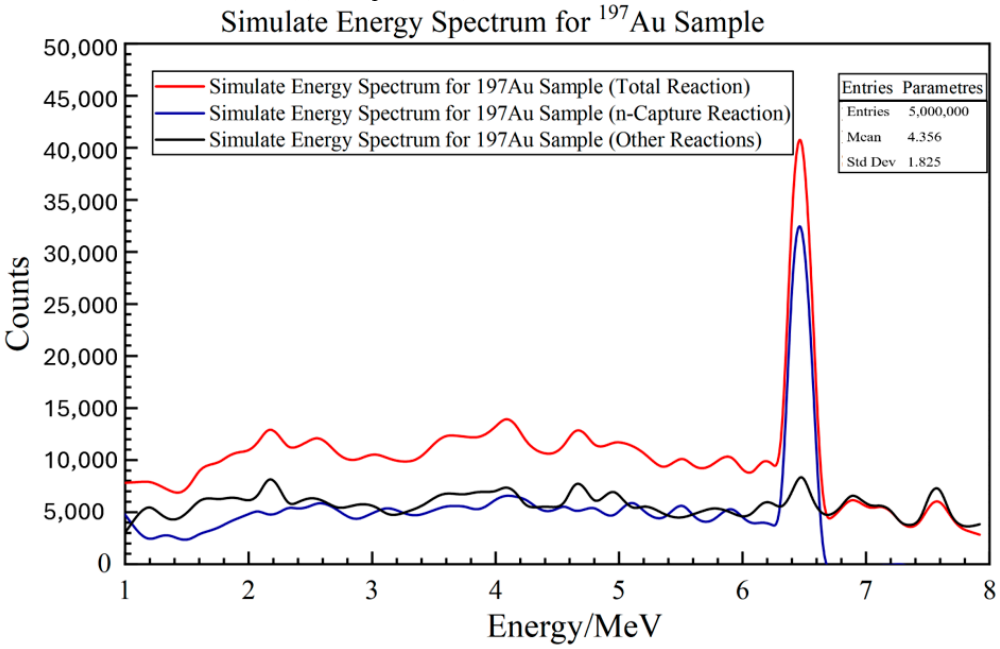

(**b**) Energy spectrum (different reaction channels)

Figure 12. Demonstrations of reaction channel discrimination.

6.2. Assistance in Evaluation of Preliminary Geometric Optimization

6.2.1. Analysis of Background

In order to support the upgrade of facilities, backgrounds can be estimated with the help of the simulation codes while comparing with the experimental results obtained. The backgrounds are defined as the differences between the total data and the effect data. With entire experimental facilities installed in the ES#2 simulation, since part of the background is produced by the interactions of scattering neutrons with the surroundings, as seen in Figure 11, a series of abnormal resonant peaks is displayed in the ToF spectrum that range from 8×10^5 ns to 1.1×10^6 ns. The preceding geometric volumes and related materials of the abnormal data are traced by the simulation codes, as shown in Figure 13.

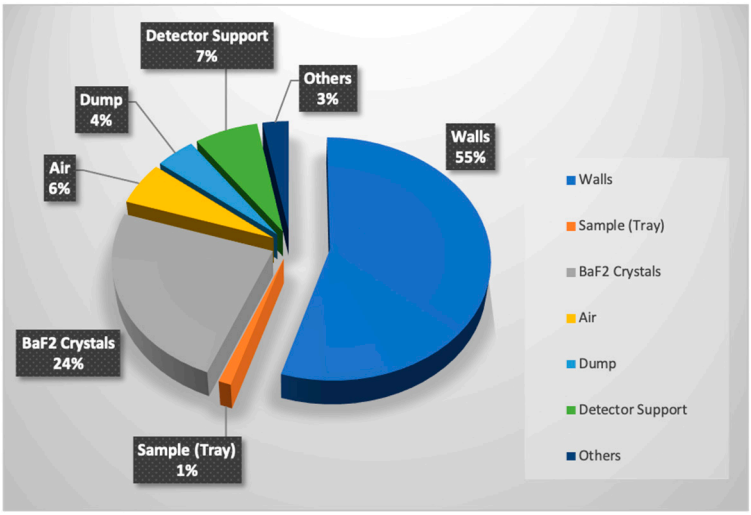

(**a**) Source of precursor geometric volume analysis

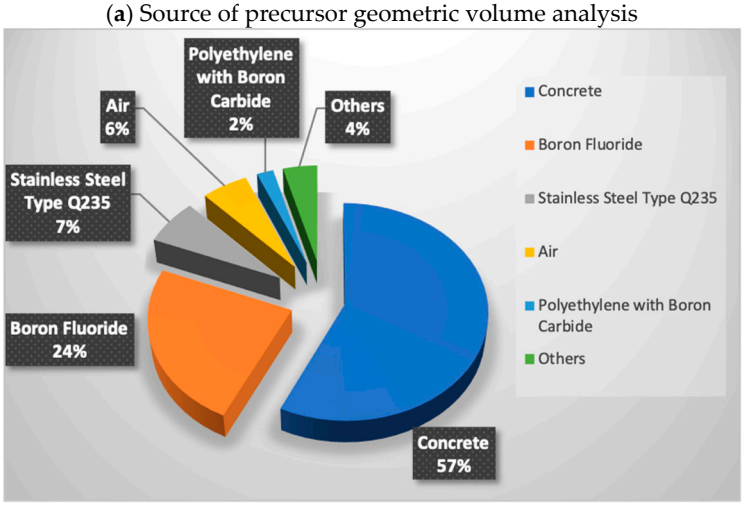

(**b**) Source of precursor material analysis

Figure 13. Demonstration of primary analysis of background.

Considering that most of the precursor origins of the background are concrete volumes (walls, ceilings, and floors), a preliminary optimization proposal could thus be made as the proposition to reduce the impact of abnormal backgrounds to isolate the scattering sub-particles caused by the wall, the ceiling, and the floor from the neutron beamline, especially in the central area where the crystal array lies.

6.2.2. Comparison of Simulation and Experimental Results

In order to verify the validity of the simulation backgrounds, two conditions are simulated: (1) under vacuum conditions, with only the BaF_2 crystals and sample reconstructed; and (2) under normal air conditions, with all geometric structures reconstructed. Theoretically, the subtraction of the two conditions could be seen as the simulated backgrounds, which are compared with the processed experimental results, as shown in Figure 14.

The simulated backgrounds compare quite favorably with the behavior of the experimental backgrounds, though the experimental backgrounds show a higher count due to either scattering due to geometrical features not included in the simulation or inaccurate cross-section values for the isotopes in the GEANT4 library. Additionally, variations in detector noise, cross-section errors, and modeling inaccuracies might contribute to the discrepancies observed. These are certainly influences affecting simulation accuracy and should be considered during the final analysis.

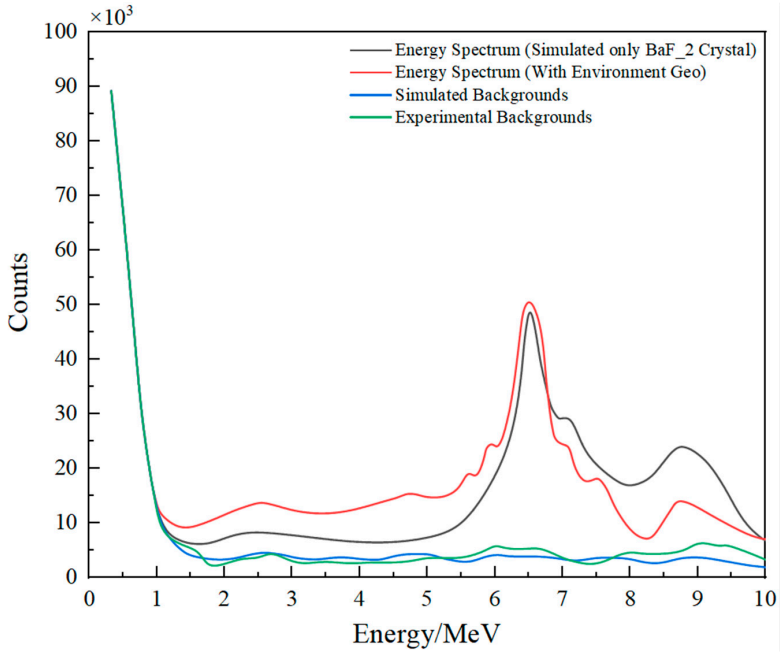

Figure 14. Background analysis and comparison.

6.2.3. Evaluation of Geometric Optimization Proposition

One potential structural optimization option is to add a vacuum tube in the central area (i.e., the area through the center of the detector array) with a ball-shaped neutron absorber outside the sample tray/support, as shown in Figure 15.

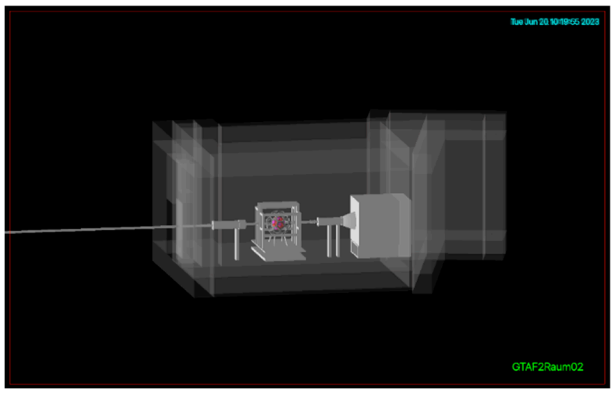

(**a**) Mass plan with the optimized structure

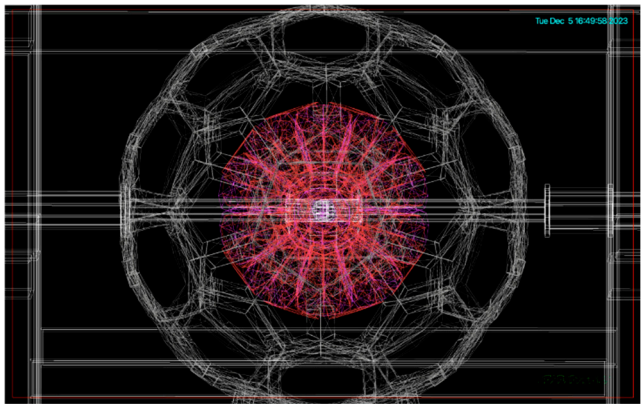

(**b**) Detail simulation of the optimization structure

Figure 15. Mass plan with the optimized structure.

The simulation results for the combination of different pipe diameters and materials are summarized in Table 5, which shows that the addition of the central vacuum pipe and the absorber outside the sample tray can significantly help to reduce the influence of the anomalous background.

Table 5. Theoretical Effect–Background ratio of simulation under different optimization conditions.

Number of Simulations	Central Pipe		Absorber Outside Sample Tray		Effect–Background Ratio
	Material	Dimension	Material	Dimension	
N_04	N/A	N/A	N/A	N/A	7.26%
N_08	Stainless Stell 304	ϕ51	Polyethylene (30% Boron Carbide)	ϕ51	15.87%
N_09	Aluminum	ϕ52		ϕ52	15.31%
N_10	Alloy 6061	ϕ55		ϕ55	16%

Obviously, the final optimization of the structure would be decided after considering more details and analysis, including the effects of in-beam γ rays at Back-n sources. Validation experiments of absorbing layers are being planned, after which all the simulated and experimental data will be verified in the very near future.

7. Summary

A Monte Carlo simulation program for GTAF based on GEANT4 toolkits is established and verified in this paper, which allows us to use it assisting the analysis of experimental data and the optimization of facilities.

The geometry of the facilities is reconstructed in great detail according to the as-built drawings and the actual layout conditions on site. Together with reasonable physics configurations and event reconstruction algorithms, the codes are tested and validated by comparing simulated with experimental data for the three types of calibration sources and two types of neutron beam sources. All of the comparison results show positive agreements, which demonstrate the reliability of the codes created.

Two types of typical application examples are presented at the end of this paper to show some common scenarios where the above codes can be applied.

More work will be done to ensure the performance of the codes and more applicable scenarios will be executed to help in data analysis and other elements of the simulation codes. While the current simulation demonstrates reliability, there is room for further improvements, such as refining background estimation for complex environments and enhancing geometric modeling to account for minor structural details.

Author Contributions: Conceptualization, C.Z. and X.R.; methodology, C.Z., G.L. and H.L.; software, H.L., Q.Z. and J.R.; validation, C.Z., G.L., X.R. and H.H.; formal analysis, C.Z., G.H. and Q.S.; investigation, C.Z., X.R., J.B. and Q.Z.; resources, C.Z., X.R. and J.W.; data curation, H.H., X.W. and M.K.; writing—original draft preparation, C.Z. and X.R.; writing—review and editing, C.Z., X.R., Z.W. and Y.L.; visualization, C.Z., H.Y., Z.W. and X.C.; supervision, X.R. and G.H.; project administration, C.Z. and X.R.; funding acquisition, X.R. and C.Z. All authors have read and agreed to the published version of the manuscript.

Funding: This project was supported by the National Natural Science Foundation of China (Nos. 11975317, 11975318, and 12275363), the Key Laboratory of Nuclear Data Foundation (No. JCKY2022201C158) and the Continuous-Support Basic Scientific Research Project (No. BJ010261223282).

Data Availability Statement: Data are contained within the article.

Conflicts of Interest: Author Chong Zou was employed by the company "China Shipbuilding Trading Co., Ltd.". The remaining authors declare that the research was conducted in the absence of any commercial or financial relationships that could be construed as a potential conflict of interest.

References

1. Wang, X.; He, G.; Zhang, Q.; Luo, H.; Xu, K.; Li, Q.; Xie, L.; Luan, G.; Ruan, X.; Zou, C.; et al. Measurement of Neutron Radiation Capture Reaction Cross Section for Rhenium. *At. Energy Sci. Technol.* **2024**, *58*, 2262–2268.
2. Farget, F.; Chomaz, P. *GANIL Scientific Annual Report 2022*; Grand Accélérateur National d'Ions Lourds: Caen, France, 2023.
3. Reifarth, R.; Lederer, C.; Käppeler, F. Neutron reactions in astrophysics. *J. Phys. G Nucl. Part. Phys.* **2014**, *41*, 053101. [CrossRef]
4. Macon, K.T. Direct Measurements of Nuclear Reactions in Hot Stellar Environments. Ph.D. Thesis, Louisiana State University and Agricultural & Mechanical College, Baton Rouge, LA, USA, 2016.
5. Ruirui, F.; Qiang, L.; Jie, B.; Yang, L.; Rong, L.; Wei, J.; Jie, R.; Qiwei, Z.; Ping, C.; Minhao, G.; et al. Detector development at the Back-n white neutron source. *Radiat. Detect. Technol. Methods* **2023**, *7*, 171–191. [CrossRef]
6. Guangyuan, L.; Jie, R.E.; Qiwei, Z.H.; Xichao, R.U.; Guozhu, H.E.; Pinjing, C.H.; Mingwei, G.U. Experiment and Simulation of Detection Efficiency of Gamma-ray Total Absorption Facility. *J. Isot.* **2022**, *35*, 273.
7. Tang, J.; Liu, R.; Zhang, G.; Ruan, X.; Wu, X.; An, Q.; Bai, J.; Bao, J.; Bao, Y.; Cao, P.; et al. Initial years' neutron-induced cross-section measurements at the CSNS Back-n white neutron source. *Chin. Phys. C* **2021**, *45*, 062001. [CrossRef]
8. Prettyman, T.H.; Feldman, W.C.; McSween, H.Y.; Dingler, R.D.; Enemark, D.C.; Patrick, D.E.; Storms, S.A.; Hendricks, J.S.; Morgenthaler, J.P.; Pitman, K.M.; et al. Dawn's gamma ray and neutron detector. In *The Dawn Mission to Minor Planets 4 Vesta and 1 Ceres*; Springer: New York, NY, USA, 2012; pp. 371–459.
9. Eberth, J.; Simpson, J. From Ge (Li) detectors to gamma-ray tracking arrays–50 years of gamma spectroscopy with germanium detectors. *Prog. Part. Nucl. Phys.* **2008**, *60*, 283–337. [CrossRef]
10. Wan, L.; Raveh, D.; Yu, T.; Zhao, D.; Korotkova, O. Optical resonance with subwavelength spectral coherence switch in open-end cavity. *Sci. China Phys. Mech. Astron.* **2023**, *66*, 274213. [CrossRef]
11. Khaliq, A.; Zhou, X.; Chai, H.; Ali, M.; Wu, H.; Gassab, O.; Liu, H.; Xiao, D.; Yang, X.G.; Du, S. Illumination Induced Negative Differential Resistance in InGaAs Avalanche Photodiode. *IEEE Access* **2024**, *12*, 50595–50604. [CrossRef]
12. Zheng, Y.; Zheng, J.; Wang, X.; Lu, Y. Gamma radiation effects on high-temperature superconducting ReBCO tape. *Supercond. Sci. Technol.* **2024**, *37*, 045013. [CrossRef]
13. Li, Q.; Yang, Y.; Wen, Y.; Zhang, G.; Xing, W. Active Gate Driver With the Independent Suppression of Overshoot and Oscillation for SiC MOSFET Modules. *IEEE Trans. Ind. Electron.* **2024**, 1–11. [CrossRef]
14. Zheng, J.; Cheng, Y.; Wang, L.; Liu, F.; Liu, H.; Li, M.; Zhu, L.A. A newly developed 10 kA-level HTS conductor: Innovative tenon-mortise-based modularized conductor (TMMC) based on China ancient architecture. *Supercond. Sci. Technol.* **2024**, *37*, 065006. [CrossRef]
15. Chen, S.; Sun, Y.; Zhang, H.; Xu, T.; Zhang, Z.; Han, Q.; Liu, T.; Zou, Y.; Cheng, Z. Mid-Infrared Hyperuniform Disordered Solids Waveguide Devices with Morphology Engineering and Wall-Network Regulation. *Laser Photonics Rev.* **2024**, 2400469. [CrossRef]
16. Copley, J.R.; Udovic, T.J. Neutron time-of-flight spectroscopy. *J. Res. Natl. Inst. Stand. Technol.* **1993**, *98*, 71. [CrossRef] [PubMed]
17. Chen, Q.; Howell, C.R.; Carman, T.S.; Gibbs, W.R.; Gibson, B.F.; Hussein, A.; Kiser, M.R.; Mertens, G.; Moore, C.F.; Morris, C. Measurements of the Neutron-Neutron Scatt. Length Using π-D Capture Reaction. *Phisical Rev. C—Nucl. Phys.* **2008**, *77*, 054002. [CrossRef]
18. Demarteau, M.; Lipton, R.; Nicholson, H.; Shipsey, I. Particle and nuclear physics instrumentation and its broad connections. *Rev. Mod. Phys.* **2016**, *88*, 045007. [CrossRef]
19. Si, D.; Xiao, S.; Qin, Y.; Xu, J.; Tian, B.; Zhang, B.; Guo, D.; Qin, Z.; Wei, X.; Hao, Y.; et al. The neutron array of the compact spectrometer for heavy ion experiments in Fermi energy region. *Nucl. Instrum. Methods Phys. Res. Sect. A Accel. Spectrometers Detect. Assoc. Equip.* **2025**, *1070*, 170055. [CrossRef]
20. Xu, X.; Fu, X.; Zhao, H.; Liu, M.; Xu, A.; Ma, Y. Three-Dimensional Reconstruction and Geometric Morphology Analysis of Lunar Small Craters within the Patrol Range of the Yutu-2 Rover. *Remote Sens.* **2023**, *15*, 4251. [CrossRef]
21. Klempt, W. Review of particle identification by time of flight techniques. *Nucl. Instrum. Methods Phys. Res. Sect. A Accel. Spectrometers Detect. Assoc. Equip.* **1999**, *433*, 542–553. [CrossRef]
22. Yu, T.; Cao, P.; Ji, X.Y.; Xie, L.K.; Huang, X.R.; An, Q.; Bai, H.Y.; Bao, J.; Chen, Y.H.; Cheng, P.J.; et al. Electronics of Time-of-Flight Measurement for Back-n at CSNS. *IEEE Trans. Nucl. Sci.* **2019**, *66*, 1095–1099. [CrossRef]
23. Xie, L.; Cao, P.; Yu, T.; Tang, X.; Jiang, Z.; An, Q.; Huang, X.; Li, C.; Li, J.; Gu, M.; et al. Real-time digital trigger system for GTAF-II at CSNS Back-n white neutron source. *J. Instrum.* **2021**, *16*, P10029.
24. Guerrero, C.; Cano-Ott, D.; Mendoza, E.; Taín, J.L.; Algora, A.; Berthoumieux, E.; Colonna, N.; Domingo-Pardo, C.; González-Romero, E.; Heil, M.; et al. Monte carlo simulation of the n_TOF total absorption calorimeter. *Nucl. Instrum. Methods Phys. Res. Sect. A Accel. Spectrometers Detect. Assoc. Equip.* **2012**, *671*, 108–117. [CrossRef]
25. Jandel, M.; Bredeweg, T.A.; Couture, A.; Fowler, M.M.; Bond, E.M.; Chadwick, M.B.; Clement, R.R.C.; Esch, E.I.; O'Donnell, J.M.; Reifarth, R.; et al. GEANT4 simulations of the DANCE array. *Nucl. Instrum. Methods Phys. Res. Sect. B Beam Interact. Mater. At.* **2007**, *261*, 1117–1121. [CrossRef]

26. Agostinelli, S.; Allison, J.; Amako, K.A.; Apostolakis, J.; Araujo, H.; Arce, P.; Asai, M.; Axen, D.; Banerjee, S.; Barrand, G.J.N.I.; et al. GEANT4—A simulation toolkit. *Nucl. Instrum. Methods Phys. Res. Sect. A Accel. Spectrometers Detect. Assoc. Equip.* **2003**, *506*, 250–303. [CrossRef]
27. Poole, C.M.; Cornelius, I.; Trapp, J.V.; Langton, C.M. A cad interface for geant4. *Australas. Phys. Eng. Sci. Med.* **2012**, *35*, 329–334. [CrossRef]
28. Gayer, D.; O'Sullivan, C.; Scully, S.; Burke, D.; Brossard, J.; Chapron, C. FreeCAD visualization of realistic 3D physical optics beams within a CAD system-model. *Millim. Submillimeter Far-Infrared Detect. Instrum. Astron. VIII* **2016**, *9914*, 745–758.
29. Apostolakis, J.; Wright, D.H.; Geant4 collaboration. An overview of the GEANT4 toolkit. *AIP Conf. Proc.* **2007**, *896*, 1–10.
30. Bečvář, F. Simulation of γ cascades in complex nuclei with emphasis on assessment of uncertainties of cascade-related quantities. *Nucl. Instrum. Methods Phys. Res. Sect. A Accel. Spectrometers Detect. Assoc. Equip.* **1998**, *417*, 434–449. [CrossRef]
31. Jie, R.; Xichao, R.; Hongqing, T.; Zhigang, G.; Hanxiong, H.; Hantao, J.; Jingyu, T.; Weiling, H. Simulation of the background of experimental end-stations and the collimator system of the CSNS back-streaming white neutron source. *Nucl. Tech.* **2014**, *37*, 100521. [CrossRef]
32. Chen, Y.; Luan, G.; Bao, J.; Jing, H.; Zhang, L.; An, Q.; Bai, H.; Cao, P.; Chen, Q.; Cheng, P. Neutron energy spectrum measurement of the Back-n white neutron source at CSNS. *Eur. Phys. J. A* **2019**, *55*, 115. [CrossRef]
33. Qi, B.; Li, Y.; Zhu, D.; Zhang, Z.; Fan, R.; Pan, J.; Feng, J.; Liu, C.; Feng, C.; Liu, J.; et al. Measurement of the neutron beam profile of the Back-n white neutron facility at CSNS with a Micromegas detector. *Nucl. Instrum. Methods Phys. Res. Sect. A Accel. Spectrometers Detect. Assoc. Equip.* **2020**, *957*, 163407. [CrossRef]
34. Matsumoto, M.; Nishimura, T. Mersenne twister: A 623-dimensionally equidistributed uniform pseudo-random number generator. *ACM Trans. Model. Comput. Simul. (TOMACS)* **1998**, *8*, 3–30. [CrossRef]
35. Martirosyan, N.; Savvidy, K.; Savvidy, G. Spectral test of the MIXMAX random number generators. *Chaos Solitons Fractals* **2019**, *118*, 242–248. [CrossRef]